Catalysis Today 138 (2008) 222–227

Contents lists available at ScienceDirect

Catalysis Today

journal homepage: www.elsevier.com/locate/cattod

Effect of structural and acidity/basicity changes of CuO–CeO_2 catalysts on their activity for water–gas shift reaction

Petar Djinović, Janez Levec, Albin Pintar *

Laboratory for Catalysis and Chemical Reaction Engineering, National Institute of Chemistry, Hajdrihova 19, P.O. Box 660, SI-1001 Ljubljana, Slovenia

ARTICLE INFO

Article history:
Available online 21 July 2008

Keywords:
Cu–Ce mixed oxide catalysts
CuO loading
Calcination temperature
Water–gas shift reaction
Surface acidity/basicity

ABSTRACT

The objective of this work was to investigate the influence of CuO loading and catalyst pretreatment procedure to derive an optimal CuO–CeO_2 catalyst for the water–gas shift reaction (WGS), and to study in detail structure– and surface acidity–activity relationships. Catalyst samples prepared by coprecipitation and a 10, 15 and 20 mol% CuO content were examined by XRD, BET and TPR/TPD analyses and subjected to pulse WGS activity tests in the temperature range of 180–400 °C. Strong structure–activity dependence in the WGS reaction was observed for all catalyst samples. It was established that increasing CuO content has a positive effect on H_2 production during the WGS reaction, due to favored CeO_2 reduction. Increasing calcination temperature on the other hand reduces the BET surface area, induced by CuO sintering and agglomeration of CeO_2 particles, resulting in a negative effect on H_2 production. Distinctive WGS activity dependence on surface acidity was observed and investigated.

1. Introduction

CuO–CeO_2 mixed oxides are gaining popularity as very active heterogeneous catalysts for various reactions, including PROX [1], the WGS reaction [2] and lower hydrocarbon transformation into synthesis gas [3,4]. The CuO–CeO_2 system exhibits activity and selectivity for CO oxidation comparable to those of commercial precious metal catalysts [5]. The simple Ce^{4+}/Ce^{3+} redox cycle leads to an outstanding oxygen storage capacity (OSC), with reversible addition and removal of oxygen in the fluorite structure of CeO_2 [6]. The strong metal–support interactions (SMSI) between Cu species and surface oxygen vacancies (catalyst redox properties) are believed to have a pronounced and positive effect on catalyst activity for the WGS reaction and other catalytic applications.

The formation of a Cu–Ce mixed oxide phase and interactions at the CuO–CeO_2 interface enable both components to be reduced and oxidized more readily. Enhanced activity in oxidation reactions is believed to be connected to the synergistic redox effect of Cu on CeO_2 and vice versa [7]. It is generally agreed that optimum catalytic properties of CuO–CeO_2 catalysts can be achieved in the presence of well-dispersed CuO species over CeO_2 nanoparticles [8]. Wang et al. [9] reported that both metallic Cu and oxygen vacancies in CeO_2 are involved in the generation of catalytically active sites for the WGS reaction on CuO–CeO_2 catalysts prepared with a modified reversed micro emulsion method. A careful balance between the redox state of CuO and CeO_2 phases is required to obtain an optimum catalytic activity, as well as to depress formation of different surface carbonate species that strongly hinder catalyst activity.

Our objective was to investigate the influence of CuO loading and catalyst pretreatment procedure to derive an optimal CuO–CeO_2 catalyst for the WGS reaction and to study structure–activity relationships. Besides the determination of catalyst activity and redox properties, samples were subjected to NH_3 pulse chemisorption/TPD analysis to obtain better understanding of surface acidity/basicity influence on catalyst performance.

2. Experimental

2.1. Synthesis of CuO–CeO_2 catalyst precursors

CuO–CeO_2 oxide catalyst precursors were prepared with a method of coprecipitation. An aqueous solution of $Na_2CO_3{\cdot}10H_2O$ was added dropwise to aqueous solutions of $Cu(NO_3)_2{\cdot}3H_2O$ and $Ce(NO_3)_3{\cdot}6H_2O$. The amount of $Cu(NO_3)_2$ solution added was calculated to yield a final 10, 15 and 20 mol% CuO in the obtained mixed oxide samples. A more detailed preparation procedure is described elsewhere [10,11]. Numbers 10, 15 and 20, when referring to catalyst samples, denote nominal mole fraction of CuO, present in those samples.

* Corresponding author. Tel.: +386 1 47 60 283; fax: +386 1 47 60 300.
E-mail address: albin.pintar@ki.si (A. Pintar).

0920-5861/$ – see front matter © 2008 Elsevier B.V. All rights reserved.
doi:10.1016/j.cattod.2008.05.032

2.2. Characterization

X-ray diffractograms were recorded on a PANalytical X'pert PRO diffractometer using Cu Kα radiation with a wavelength of 0.15406 nm. The scanned 2θ range was between 6 and 85° with 0.034° increments and 1 s measuring time at each increment.

Prior to TPR and TPD tests, catalyst precursors were calcined *in situ* in synthetic air (20.5% O_2/N_2). Single-point BET (30% N_2/He), H_2-TPR and H_2-TPD measurements were performed using a Micromeritics AutoChem II 2920 apparatus on 250 mg of catalyst samples, calcined in the temperature range from 400 to 750 °C. TPR analysis was performed in a 50 ml/min (GHSV = 9400 h^{-1}) stream of 5% H_2/Ar as a reducing agent. The samples were heated from −20 to 400 °C with a 5 °C/min ramp during analysis. The samples subjected to TPD analysis were investigated in the temperature range of −20 to 700 °C with a 5 °C/min heating ramp in a flow of Ar with a 50 ml/min flow rate. CuCe 10, CuCe 15 and CuCe 20 samples were subjected to pulse NH_3 (10% NH_3 in He) chemisorption at 90 °C after sample calcination in synthetic air (50 ml/min) and reduction at 400 °C in 5% CO/He. Afterwards, CO_2/NH_3-TPD profiles were obtained while increasing sample temperature from 90 to 650 °C in a He stream with a 10 °C/min ramp and recorded with a TCD detector and mass spectrometer. CuO dispersion was determined by pulse N_2O decomposition at 90 °C with 10% N_2O/He on calcined (synthetic air), reduced (5% H_2/Ar) and degassed (He) catalyst samples. Decomposition of N_2O and formation of N_2 were monitored with a Pfeiffer Vacuum ThermoStar mass spectrometer.

2.3. Catalytic activity

Catalyst samples (≈30 mg) were placed on top of loosely packed quartz wool at the bottom of a U-shaped quartz test tube (designed to minimize channeling effects), which was inserted into an electric furnace of the Micromeritics' AutoChem apparatus. Prior to all activity tests carried out at atmospheric pressure, the catalyst precursors were calcined *in situ* in synthetic air (20.5% O_2/N_2) for 60 min at individual calcination temperatures and then reduced in a 50 ml/min flow of 5% CO/He at 400 °C for 90 min. During activity tests, pulses of saturated water vapor at 75 °C in He were produced in a calibrated vapor generator (0.53 ml STP) and injected into the CO/He stream (GHSV = 33,000 h^{-1}). Sample temperature was gradually raised from 180 to 400 °C in 25 °C increments. Four pulses of water vapor were dosed at each reaction temperature in order to investigate repeatability and to obtain more reliable results. WGS reaction products as well as unconverted reactants were continuously recorded with a mass spectrometer.

3. Results and discussion

With increasing calcination temperature of CuCe samples, XRD peaks become more narrow and intense as a result of CeO_2 particle sintering, ordering of structure and crystallite growth (Table 1). CeO_2 crystallites grow by almost two orders of magnitude in the applied range of calcination temperatures. A slight shift of characteristic peaks toward higher 2θ angles occurs for CuCe 15 and CuCe 20 samples. This shift could mean a unit cell size reduction (Table 1), as Cu integration into the CeO_2 lattice occurs and sample structure and chemical composition approach the thermodynamically most stable state [7]. This shift is not observed for CuCe 10 samples, possibly because of lower Cu content. The lack of CuO peaks in diffractograms at lower calcination temperatures suggests that CuO particles are either amorphic, too small to be detected by XRD or partly integrated into CeO_2, forming a solid solution. Significant BET surface area reduction is primarily determined with the applied calcination temperature and much less with CuO loading (Table 1). The actual Cu content was determined with inductively coupled plasma-atomic emission spectroscopy (ICP-AES) and equals 11.0 mol% for CuCe 10, 18.5 mol% for CuCe 15 and 29.0 mol% for the CuCe 20 catalyst sample. These values were used to calculate the extent of partial CeO_2 reduction (Table 1).

3.1. H_2-TPR and TPD analyses

In comparison to pure CuO, reduction of CuO–CeO_2 species in intimate contact, as present in tested catalysts, takes place at much lower temperatures with complex reduction peaks, which change with increasing calcination temperature and CuO loading. The strong metal oxide–support interactions between CuO and CeO_2

Table 1
Average crystallite size (d_{CeO_2}), CeO_2 cell parameter size, BET surface area, TPR and TPD data, partial CeO_2 reduction, CuO dispersion (D_{CuO}) values for CuCe 10, 15 and 20 samples calcined at various temperatures

Sample	d_{CeO_2} (nm)	Ceria (1 1 1) cell parameter (nm)	BET surface area (m^2/g)	TPR (ml H_2/g) (STP)	TPD (ml H_2/g) (STP)	[a]Consumption of H_2 for CeO_2 reduction (ml H_2/g) (STP)	CeO_2 partial reduction (%)	CuO dispersion (%)
CuCe 10 400	7.4	0.5403	52.4	35.9	7.9	14.3	22.5	31.2
CuCe 10 450	8.6	0.5411	43.4	30.6	6.8	10.0	15.7	30.2
CuCe 10 500	10.1	0.5414	33.2	29.3	6.4	9.2	14.4	32.7
CuCe 10 550	12.2	0.5410	22.1	24.6	3.9	7.0	10.9	19.9
CuCe 10 600	19.9	0.5415	9.9	23.7	2.8	7.2	11.3	4.5
CuCe 10 650	34.2	0.5413	7.3	20.8	1.1	6.0	9.4	0.3
CuCe 10 750	421.4	0.5413	4.7	18.5	0.7	4.0	6.3	0.1
CuCe 15 400	7.5	0.5410	53.9	48.1	5.9	20.9	34.7	12.9
CuCe 15 450	9.3	0.5412	40.2	42.7	4.4	17.0	28.2	8.4
CuCe 15 550	29.2	0.5410	8.3	33.5	1.2	11.0	18.3	4.9
CuCe 15 650	144.0	0.5408	6.0	33.3	0.5	11.5	19.1	1.0
CuCe 15 750	184.1	0.5403	4.4	32.1	0.3	10.5	17.4	1.0
CuCe 20 400	7.4	0.5411	35.3	68.9	5.7	34.0	60.0	8.5
CuCe 20 450	8.3	0.5411	30.3	65.6	4.9	31.6	55.7	7.8
CuCe 20 500	9.6	0.5411	28.5	68.3	4.3	34.8	61.4	6.1
CuCe 20 550	13.9	0.5407	14.6	59.3	2.9	27.3	48.2	1.9
CuCe 20 650	110.3	0.5412	9.5	57.8	0.2	28.5	50.2	0.9
CuCe 20 750	66.9	0.5399	7.0	56.8	0.3	27.3	48.2	0.3

[a] The amount of H_2 used for partial CeO_2 reduction was obtained by subtracting H_2-TPD and the amount of H_2 needed for complete CuO reduction from the overall amount of H_2 consumed during H_2-TPR analyses.

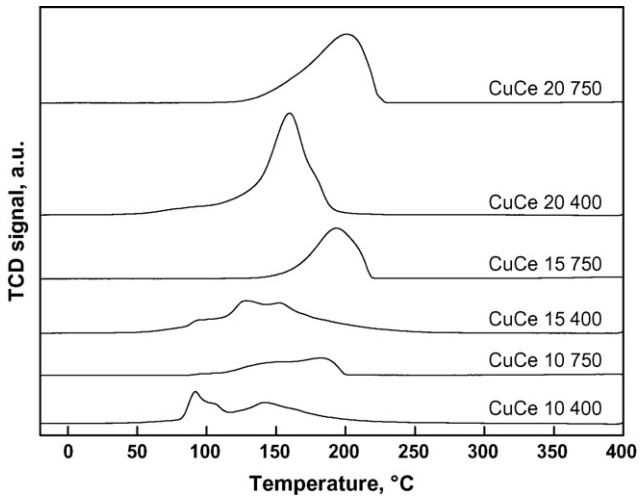

Fig. 1. Comparison of H_2-TPR reduction profiles.

are believed to lead to an electron transfer between the oxides, causing a decrease in their individual reduction temperatures [5,12] and contribute to the complexity of reduction peaks. As illustrated in Fig. 1, CuCe 10 reduction peaks in the lower temperature region (≈100 °C) belong to the reduction of well-dispersed amorphous and crystalline CuO particles strongly interacting with CeO_2, and partial surface CeO_2 reduction at the Cu–Ce interface [13]. Peaks in the higher temperature region (≈150 °C and above) belong to bulk CuO reduction and H_2 adsorption on the catalyst surface which does not contribute to reduction steps. With increasing calcination temperature, contributions of particular peak areas belonging to different-sized surface species change: (i) at lower calcination temperatures (400 and 450 °C), peaks in the 100 °C region show the greatest intensity; (ii) peaks belonging to bulk CuO reduction exhibit increased intensity at higher calcination temperatures. Compared to well-dispersed CuO, it is believed that the specific contact area of bulk CuO with the support is greatly reduced, which implies that SMSI are thus less pronounced, resulting in reduction at higher temperatures. The amount of overall H_2 used for catalyst reduction decreases drastically with increasing calcination temperature, most evidently when calcination temperature reaches 750 °C. Since the overall H_2 consumption still surpasses the one needed for complete Cu^{2+} to Cu^0 reduction, we believe that complete CuO reduction occurs in all tested samples, but CeO_2 is reduced to a lesser extent. Since CeO_2 reduction occurs primarily at the CuO–CeO_2 interface, CuO sintering and coalescence (confirmed by XRD analysis and N_2O decomposition) reduce the number of CuO–CeO_2 junctures, resulting in fewer "active sites" for CeO_2 reduction. Partial CeO_2 reduction is the lowest for CuCe 10 samples (Table 1). CeO_2 crystallite size also has a profound effect on its reduction extent, which drops significantly with increasing calcination temperature. Considering the temperature region in which the catalyst reduction occurs (Fig. 1), final CuO and CeO_2 reduction extent is attained, leaving catalyst oxidation states constant during subsequent WGS activity tests.

The higher Cu content of CuCe 15 catalysts denotes the presence of larger CuO particles, as lower values of CuO dispersion were measured. When comparing the H_2 amounts used for partial CeO_2 reduction, we can again see that these values drop continuously with increasing calcination temperature. However, a comparison of values in Table 1 demonstrates that the extent of partial CeO_2 reduction increases by increasing CuO content from nominal 10 to 15 mol%, probably through enhanced formation of the CuO–CeO_2 interface.

The listed values of CuO dispersion in Table 1 confirm that higher CuO content in CuCe 20 samples results in the presence of large CuO particles, which are correspondingly reduced at higher temperatures. This is the main cause of inferior TPR peak intensity at reduction temperatures around 100 °C, compared to samples with a lower CuO content. A temperature gap of CuCe 20 catalyst reduction in the measured TPR profiles exhibits a similar shift into the higher temperature region with increasing calcination temperature as the samples with the lower CuO content. Since CeO_2 crystallite size rises by almost two orders of magnitude in the inspected temperature region, it is possible that H_2 penetration into CeO_2 crystallites is hindered because of significantly reduced and accessible specific surface area. H_2 diffusion into the CeO_2 lattice, as well as lattice oxygen diffusion to the CeO_2 surface governs the extent of CeO_2 reduction [14]. Partial CeO_2 reduction of CuCe 20 samples drops from 60 to approximately 48%, as calcination temperature rises from 400 to 750 °C and is the highest among all tested samples (Table 1).

The amount of desorbed H_2 from calcined and H_2-reduced samples drops with increasing CuO loading and calcination temperature, indicating that the CeO_2 surface is primarily responsible for H_2 adsorption. Sample sintering and consequently a lower specific surface area result in a decreased amount of adsorbed H_2. As listed in Table 1, a negligible amount of H_2 is adsorbed on samples calcined at 650 °C and above.

3.2. WGS activity tests

WGS activity data of CuCe catalyst samples calcined at various temperatures are presented in Fig. 2. As expected, typical S-shaped curves were obtained, which show that the activity of the examined solids increases with an increase in reaction temperature and levels off at higher temperatures due to the WGS reaction equilibrium and occurrence of methanation reactions. Experimental error of data points depicted in Fig. 2 was below ±4.7%. Among CuCe 10 catalysts (Fig. 2a), the highest H_2 production was observed over the CuCe 10 550 sample, with H_2 selectivity of 74% at approximately 95% water conversion. Since methane production was the only side product detected, the given values of H_2 selectivity reflect the extent of CH_4 formation. A comparison of data measured, for example, over CuCe 10 400 and CuCe 10 550 samples provides a proof that methanation reactions take place in the investigated catalytic system. In comparison to the catalyst sample calcined at 550 °C, maximum selectivity towards H_2 of about 34% was obtained over the CuCe 10 400 catalyst. Reverse WGS reaction, resulting in lower H_2 production over CuCe 10 samples calcined at 400 and 450 °C was ruled out, because water conversion up to 100% was measured. One can see in Fig. 2a that in principle H_2 production over CuCe 10 samples decreases with an increase in calcination temperature. WGS activities of catalyst samples calcined at 650 and 750 °C were lowest of all (49 and 27% H_2O conversion with roughly 35% selectivity towards H_2). However, in comparison to other solids H_2 production increased drastically for catalyst samples calcined at 550 and 600 °C. This behavior cannot be attributed to modifications of textural properties, since no changes were observed apart from particle growth (Table 1), which should have a negative influence on activity at elevated calcination temperatures. No unexpected results were obtained by H_2-TPR and TPD analyses at the above mentioned calcination temperatures, since the extent of CeO_2 reduction which contributes considerably to the WGS activity of CuO–CeO_2 solids [15] decreases with an increase of calcination temperature (Table 1). The most probable reason for the increase in catalyst activity and hindrance of methanation reactions, resulting in a higher H_2 yield is in our opinion the surface acidity/basicity change occurring when CuCe 10 samples were calcined at 550 and 600 °C (Fig. 3). Surface acidity/

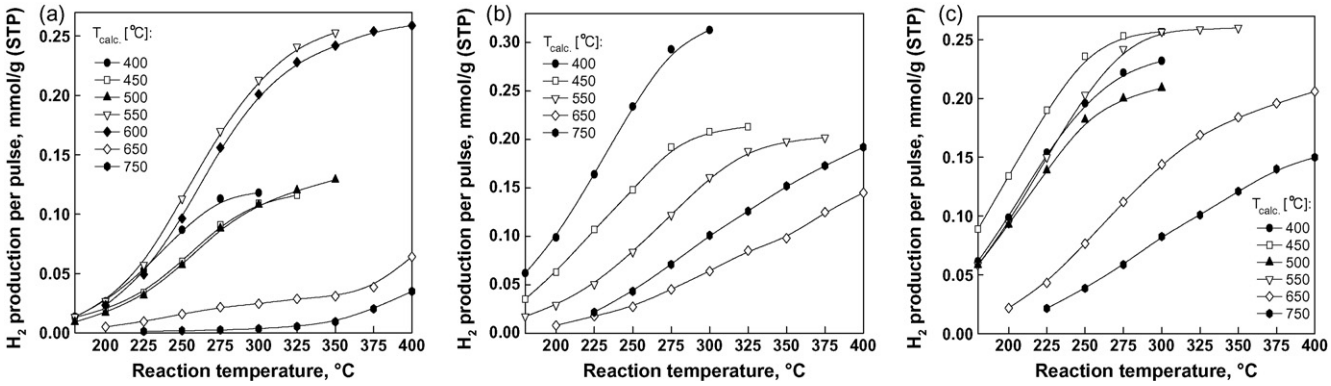

Fig. 2. WGS activity as a function of reaction temperature of (a) CuCe 10, (b) CuCe 15 and (c) CuCe 20 catalyst samples calcined at different temperatures.

basicity changes are caused by stabilization of coordinatively unsaturated CuO and CeO_2 planes via reconstruction phenomena or adsorption of surrounding gas molecules. The presence of carbonate-like species on the surface of CuO–CeO_2 mixed oxides was confirmed by means of TPD analysis following the calcination and reduction of catalyst precursors in synthetic air and CO atmosphere, respectively. This analysis (Fig. 3) shows noticeable quantities of CO_2 desorbed at temperatures above 430 °C, with a peak maximum at around 620 °C. Carbonate-like species originate from reducing CO gas interaction with surface oxygen species. It is reported by Hilaire et al. [16] that the formation of carbonates is favored in solids containing CeO_2. Assuming that CO_2 was bound preferentially to CeO_2 during the CO reduction step (which is reasonable due to its abundance), TPD analysis shows that about 1.5 mol% of CeO_2 was in the form of $Ce(CO_3)_2$ in the CuCe 10 550 sample. Gamarra et al. [17] also report the presence of monodentate, bidentate and hydrogen carbonate species on the CuO–CeO_2 surface, which can strongly influence both redox as well as surface acidic properties.

The results of surface acidity determination with pulse NH_3 chemisorption/TPD analysis are presented in Fig. 3b for CuCe 10, CuCe 15 and CuCe 20 catalysts (error below ±10%). Interestingly, one can see that both CO_2 desorption from calcined and CO-reduced catalyst samples, and NH_3 desorption from fresh catalyst samples result in similar dependencies as a function of calcination temperature. On the basis of this observation, we can propose that calcination temperature and catalyst reduction conditions (i.e. incorporation of CO_2 into the catalyst structure during the CO reduction step) determine the distribution of acidic/basic centers on the surface of CuO–CeO_2 solids. It was established during the NH_3-TPD analysis that the amount of adsorbed NH_3 per unit of surface area reaches a maximum at calcination temperature of 550 °C for CuCe 10 (Fig. 3b), because of the maximum surface acidity achieved at this specific calcination temperature. The temperature region in which NH_3 desorption occurs (100–220 °C with a maximum at 170 °C, Fig. 3a) is constant for all tested samples, indicating changes only in the number of acid sites, not in their strength. No evidence was observed in this study to correlate the measured catalytic activity for the WGS reaction with changes in CuO dispersion. However, a clear correlation was found between the amounts of desorbed NH_3, i.e. catalyst surface acidity, and WGS activity, regardless of CuO content and calcination temperature. Increased surface acidity proved to be beneficial for CO adsorption, which might enhance the overall WGS reaction rate over CuO–CeO_2 catalysts and thus increase H_2 yield. To conclude, since CO acting as a reactant in the investigated process is a weak base, the obtained results could imply higher tendency for CO adsorption on the CuCe 10 550 catalyst surface and consequently higher CO afflux to the catalyst surface during the WGS reaction, explaining the observed rise in catalyst activity (Fig. 2a). In turn, acidic character of the CuCe 10 550 catalyst surface enables simple CO_2 desorption, leaving behind free active sites for CO and water vapor adsorption in subsequent reaction cycles.

As shown in Fig. 2b, WGS activity of CuCe 15 samples decreases continuously with increasing calcination temperature as could be expected, with the sample calcined at 400 °C being the most active. CuCe 15 samples calcined at 400, 450 and 550 °C all achieved total H_2O conversion, with CuCe 15 400 exhibiting the highest H_2 selectivity (94%). Samples calcined at 650 and 750 °C show WGS activity in reverse order from the expected one; this could again be attributed to a higher surface acidity of the CuCe 15 750 sample

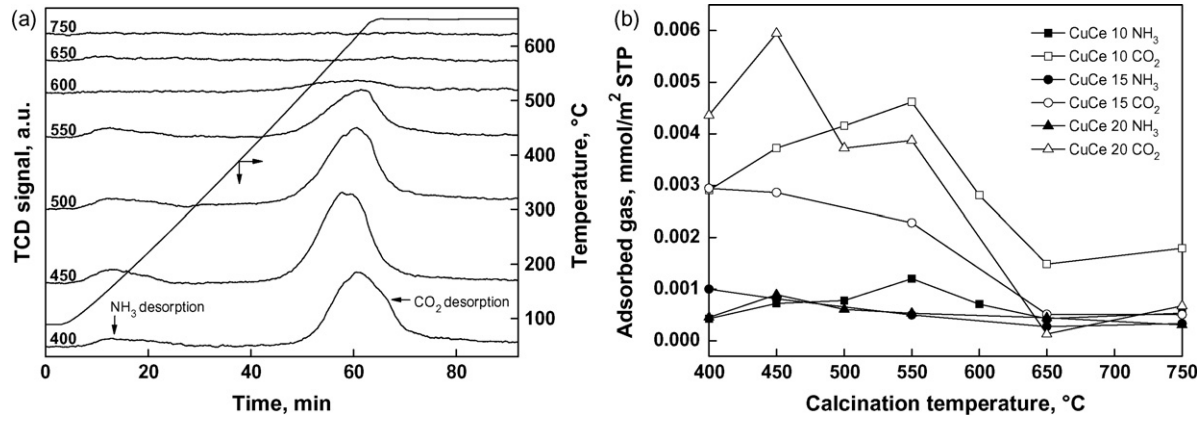

Fig. 3. (a) CuCe 10 CO_2 and NH_3-TPD curves as a function of calcination temperature and (b) amounts of desorbed NH_3 and CO_2 over CuCe 10, CuCe 15 and CuCe 20 catalysts as a function of calcination temperature.

(Fig. 3b). Higher calcination temperature and sample sintering exhibit a smaller negative effect on catalyst activity for samples with higher CuO loading [18], probably because of a higher overall CuO–CeO_2 interface area (Table 1), which is believed to constitute active sites for the WGS reaction [15].

Catalyst surface rearrangements, when subjected to different calcination temperatures, have a pronounced effect on WGS activity, which is also observed for CuCe 20 samples (Fig. 2c). A comparison of data listed in Fig. 3b suggests that changes in surface acidity of samples calcined at 450 and 550 °C, respectively, have an overpowering positive effect on WGS activity over sintering and extent of surface CeO_2 reduction [15,19]. An overall comparison of H_2 yields (Fig. 2) clearly shows that increasing CuO content in CuO–CeO_2 catalysts has a positive effect on their WGS reaction activity. Increasing the CuO–CeO_2 interface area plays a decisive role in the formation of optimum surface composition, since CeO_2 crystallite size (Table 1) is very similar for all samples at lower calcination temperatures (up to 550 °C). This is in agreement with the results of our previous study [15], where we proposed that WGS activity of CuO–CeO_2 catalysts synthesized by various methods is linearly proportional to the extent of surface CeO_2 reduction.

CuCe 10, CuCe 15 and CuCe 20 catalysts calcined at 400 °C all achieved complete water conversion (≈100%), but the amounts of produced H_2 differed considerably (Fig. 2), due to H_2 selectivity variations, which were probably a consequence of optimal CuO and CeO_2 morphology formation, as well as distribution of acidic/basic sites, determined by both CuO content and calcination temperature.

3.3. Correlating trends in WGS activity of CuO–CeO_2 catalysts

It was shown in our previous study [15] that the WGS activity of CuO–CeO_2 catalysts is related to the following parameters: (i) reducibility of the surface CeO_2 layer; (ii) active surface area, which is proportional to the average CeO_2 crystallite size (d_{CeO_2}). Both parameters are strongly influenced by the catalyst preparation procedure. Based on these facts, we can propose an equation to predict a trend of WGS activity of the examined CuCe catalysts, which reads:

$$\text{WGS trend activity} = \text{PCR}\left(\frac{1}{d_{CeO_2}}\right)^2 \quad (1)$$

The term PCR stands for the amount of H_2 consumed for partial CeO_2 reduction, while the second right-hand term in Eq. (1) represents a measure for the Cu–Ce interface accessible to reactants. Since oxidation of adsorbed CO to CO_2 with surface oxygen is regarded as the rate determining step in catalyzed WGS reaction over CuO–CeO_2 [20], the extent of partial CeO_2 reduction is thus of crucial importance when it comes to oxygen species availability for CO oxidation. The greater the extent of partial CeO_2 reduction achieved during the catalyst activation, more surface CeO_2 species take an active part in CO oxidation, thus providing an abundance of oxygen species for the reaction. This is in agreement with a recent *in situ* investigation of WGS reaction over Cu–CeO_2 catalysts, which shows that both metallic Cu and oxygen vacancies in CeO_2 are involved in the generation of active sites [9].

Experimental (T = 250 °C) and trend WGS activities are depicted for different CuO loadings and calcination temperatures in Fig. 4. Fairly good agreement between the measured and the calculated trends was obtained. The WGS activity rise of CuCe 10 550 and 600 samples cannot be sufficiently explained by means of Eq. (1), since the activity increase is not connected only to variations in CeO_2 crystallite size and CeO_2 reduction extent, but is considerably influenced by the modifications of surface acidic properties, and consequently with the extent of methanation reactions. On the other hand, WGS activity of CuCe 15 samples can be well predicted by means of Eq. (1) over a wide range of calcination temperatures (Fig. 4b). Similarly to CuCe 10 samples, calcination at 450 and 550 °C again caused a rise in the WGS activity of CuCe 20 samples, although in this case the increase was less pronounced (Fig. 4c). As discussed above, reasons for such behavior can in our opinion be attributed to a different distribution of acidic/basic centers resulting from the treatment at afore-mentioned calcination temperatures. To conclude, results in Fig. 4 show that Eq. (1), requiring data from XRD and H_2-TPR/TPD analyses, provides a useful and simple tool for estimating trends in WGS activity among CuO–CeO_2 mixed oxide catalysts with various CuO loadings and calcined in a wide range of temperatures. However, one should be aware that Eq. (1) provides reliable predictions only for solids with similar surface acidic/basic properties.

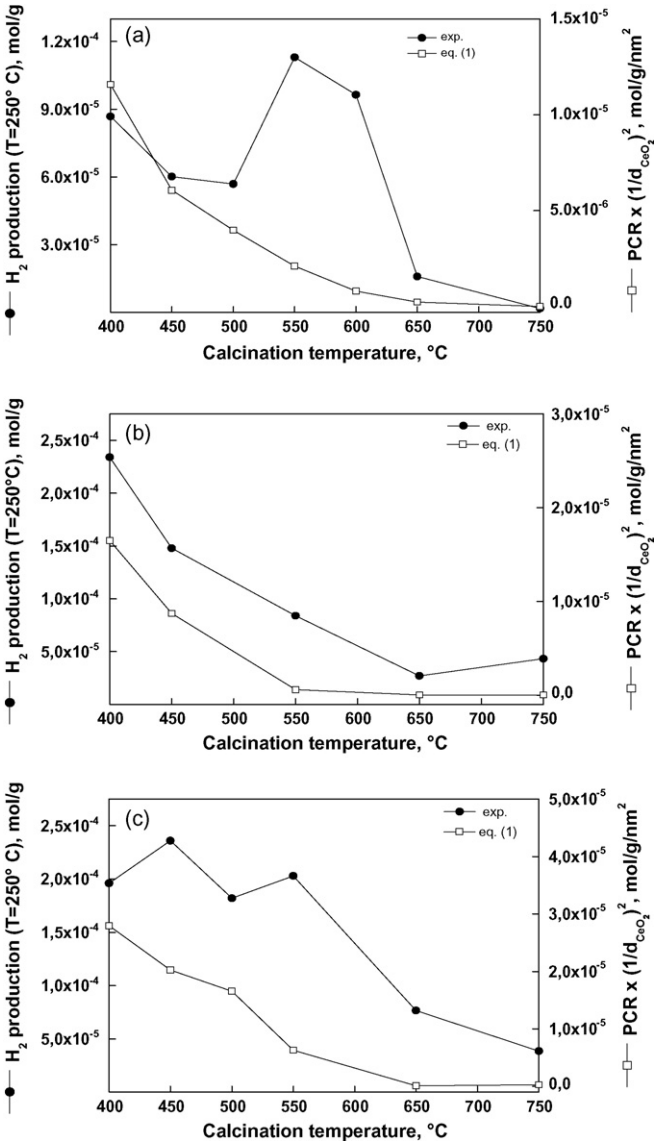

Fig. 4. Measured vs. predicted trends of H_2 yields for (a) CuCe 10, (b) CuCe 15 and (c) CuCe 20 samples.

4. Conclusions

Severe sintering of CuO–CeO_2 catalysts with various CuO loadings and synthesized by the coprecipitation method, was observed with an increase of calcination temperature. The extent of

solid solution formation depends on calcination temperature and CuO loading, as evidenced from XRD results, being more prominent for samples with a higher CuO content. TPR results reveal complex reduction profiles of Cu–Ce mixed oxide catalysts, especially those with the lowest CuO content. Both nanosized and bulk-like CuO species are reduced at lower temperatures compared to pure CuO, because of strong redox interactions with CeO_2. Surface CeO_2 reduction drops after high temperature treatment because of diffusional hindrances and fewer CuO–CeO_2 junctures present. Catalyst samples with higher CuO content exhibit higher WGS reaction activity. Contrary to that, higher calcination temperature, which results in severe CeO_2 crystallite sintering and merging of fine CuO particles, negatively affects WGS activity. The reducibility of surface CeO_2 and the active surface of the Cu–Ce interface are the prevailing factors which determine the WGS activity of CuO–CeO_2 catalysts. The results obtained in this study suggest that increased surface acidity enhances the number of adsorbed CO species on the catalyst surface. Changes in surface acidity/basicity occur with increased calcination temperature and exhibit the most pronounced effect on the WGS activity of catalysts with 10 mol% CuO loading.

Acknowledgement

The authors gratefully acknowledge the financial support of the Ministry of Education, Science and Technology of the Republic of Slovenia through Research program No. P2-0152.

References

[1] A. Martínez-Arias, A.B. Hungria, G. Munera, D. Gamarra, Appl. Catal. B 65 (2006) 207.
[2] G. Jacobs, S. Khalid, P.M. Patterson, D.E. Sparks, B.H. Davis, Appl. Catal. A 268 (2004) 255.
[3] S. Zhao, R.J. Gorte, Appl. Catal. A 277 (2004) 129.
[4] A. Trovarelli, C. de Leitenburg, M. Boaro, G. Dolcetti, Catal. Today 50 (1999) 353.
[5] P. Zimmer, A. Tschöpe, R. Birringer, J. Catal. 205 (2002) 339.
[6] W. Shan, W. Shen, C. Li, Chem. Mater. 15 (2003) 4761.
[7] W.-P. Dow, Y.-P. Wang, T.-J. Huang, Appl. Catal. A 190 (2000) 25.
[8] H. Chen, H. Zhu, Y. Wu, F. Gao, L. Dong, J. Zhu, J. Mol. Catal. A 255 (2006) 254.
[9] X. Wang, J.A. Rodriguez, J.C. Hanson, D. Gamarra, A. Martínez-Arias, M. Fernández-García, J. Phys. Chem. B 110 (2006) 428.
[10] A. Pintar, J. Batista, S. Hočevar, J. Colloid Interf. Sci. 285 (2005) 218.
[11] S. Hočevar, J. Batista, J. Levec, J. Catal. 184 (1999) 39.
[12] S. Patel, K.K. Pant, Chem. Eng. Sci. 62 (18–20) (2007) 5436.
[13] X. Tang, B. Zhang, Y. Li, Y. Xu, Q. Xin, W. Shen, Appl. Catal. 288 (2005) 116.
[14] Lj. Kundakovic, M. Flytzani-Stephanopoulos, Appl. Catal. A 171 (1998) 13.
[15] A. Pintar, J. Batista, S. Hočevar, J. Colloid Interf. Sci. 307 (2007) 145.
[16] S. Hilaire, X. Wang, T. Luo, R.J. Gorte, J. Wagner, Appl. Catal. B 215 (2001) 271.
[17] D. Gamarra, G. Munuera, A.B. Hungría, M. Fernández-García, J.C. Conesa, P.A. Midgley, X.Q. Wang, J.C. Hanson, J.A. Rodríguez, A. Martínez-Arias, J. Phys. Chem. C 111 (2007) 11026.
[18] F. Marino, C. Descorme, D. Duprez, Appl. Catal. B 58 (2005) 175.
[19] M. Xue, X. Gu, J. Chen, H. Zhang, J. Shen, Thermochim. Acta 434 (2005) 50.
[20] N.A. Koryabkina, A.A. Phatak, W.F. Ruettinger, R.J. Farrauto, F.H. Ribeiro, J. Catal. 217 (2003) 233.